1 # Unexpectedly high concentrations of atmospheric mercury

2 # species in Lhasa, the largest city on the Tibetan Plateau

3 Huiming Lin[1], Yindong Tong[2,3*], Long Chen[4], Chenghao Yu[5], Zhaohan Chu[1], Qianru

4 Zhang[1], Xiufeng Yin[6], Qianggong Zhang[7,8], Shichang Kang[6,8], Junfeng Liu[1], James

5 Schauer[9,10], Benjamin de Foy[11], Xuejun Wang[1**]

6 1. MOE Laboratory of Earth Surface Processes, College of Urban and Environmental Sciences, Peking

7 University, Beijing 100871, China;

8 2. School of Science, Tibet University, Lhasa 850000, China

9 3. School of Environmental Science and Engineering, Tianjin University, Tianjin, 300072, China;

10 4. School of Geographic Sciences, East China Normal University, Shanghai 200241, China;

11 5. Key Laboratory of Microbial Technology for Industrial Pollution Control of Zhejiang Province,

12 College of Environment, Zhejiang University of Technology, Hangzhou 310014, China

13 6. State Key Laboratory of Cryospheric Science, Northwest Institute of Eco-Environment and Resources,

14 Chinese Academy of Sciences, Lanzhou 730000, China

15 7. Key Laboratory of Tibetan Environment Changes and Land Surface Processes, Institute of Tibetan

16 Plateau Research, Chinese Academy of Sciences, Beijing, 100101, China;

17 8. CAS Center for Excellence in Tibetan Plateau Earth Sciences, Beijing, 100085, China;

18 9. Department of Civil and Environmental Engineering, University of Wisconsin-Madison, Madison, WI,

19 USA;

20 10. Wisconsin State Laboratory of Hygiene, University of Wisconsin-Madison, WI, USA;

21 11. Department of Earth and Atmospheric Sciences, Saint Louis University, St. Louis, MO, 63108, USA

22 **Correspondence:**

23 *Xuejun Wang (wangxuejun@pku.edu.cn) **Yindong Tong (yindongtong@tju.edu.cn)

24

25 **Abstract**

26 Lhasa City is located in the central Tibetan Plateau and is the most densely populated area. As

27 the first continuous monitoring of atmospheric mercury (Hg) species in a city on the Tibetan Plateau,

28 our monitoring in Lhasa showed that the concentrations of gaseous elemental Hg (GEM), gaseous

29 oxidized Hg (GOM), and particle-bound Hg (PBM) during subsequent of the Indian Summer

30 Monsoon (S-ISM) period were 2.73 ± 1.48 ng m^{-3}, 38.4 ± 62.7 pg m^{-3}, and 59.1 ± 181.0 pg m^{-3},

31 respectively. During the Westerly Circulation (WEC) period, the GEM, GOM and PBM

32 concentrations were 2.11 ± 2.09 ng m^{-3}, 35.8 ± 43.3 pg m^{-3}, and 52.9 ± 90.1 pg m^{-3}, respectively.

33 The atmospheric Hg species concentrations were higher than those of previous monitoring on the

34 Tibetan Plateau and other provincial capitals in China. Typical high-value occurrence processes

35 were studied to investigate random events with high atmospheric Hg concentrations in Lhasa.

36   Combustion event nearby or further away may be the main contributor of the high-concentration

37   events. The lowest GEM concentrations occurred in the afternoon and persistently high

38   concentrations were observed at night. The changes in GEM concentrations were consistent with

39   the trends of other pollutant concentrations and contradictory to those of the wind speed. The high

40   GEM concentrations at night can be attributed to the lower boundary layer height and lower wind

41   speed. For both GOM and PBM, higher GOM concentrations occurred during the day and PBM

42   during the night. The results of the principal component analysis indicated that local sources and

43   wind speed are important factors influencing atmospheric Hg concentrations in Lhasa. The

44   trajectory simulation showed that the source of the GEM in Lhasa gradually shifted from the south

45   to the west of Lhasa from the S-ISM to the WEC periods, while both the southern and western

46   sources were important in the late WEC period. The concentrations and change patterns of Hg

47   species in Lhasa were significantly different than those at other monitoring sites on the Tibetan

48   Plateau. Monitoring Hg species in Lhasa shows the possible maximum anthropogenic influences on

49   the Tibetan Plateau and demonstrates the dramatic effect of wind on changes in urban atmospheric

50   Hg concentrations.

51

52   **1.   Introduction**

53   Mercury (Hg) has received worldwide attention owing to its high toxicity and bioaccumulation.

54   Atmospheric mercury (Hg) exists in three different forms: atmospheric gaseous elemental Hg

55   (GEM), gaseous oxidized Hg (GOM), and particle-bound Hg (PBM) (Selin, 2009). They exhibit

56   different behaviors in the environment owing to their various chemical properties (Selin,

57   2009;Travnikov et al., 2017;Lindberg and Stratton, 1998;Seigneur et al., 2006). Many established

58   monitoring networks for atmospheric Hg exist in North America and Europe (Stylo et al., 2016)

59   including the Atmospheric Mercury Network (AMNet; Gay et al., 2013), the Global Mercury

60   Observation System (GMOS; Sprovieri et al., 2013;Sprovieri et al., 2016), the Canadian

61   Atmospheric Mercury Network (CAMNet; Kellerhals et al., 2003), and the Arctic Monitoring

62   Assessment Programme (AMAP; https://mercury.amap.no/) (Gay et al., 2013;Sprovieri et al.,

63   2013;Sprovieri et al., 2016;Kellerhals et al., 2003). They have been operating for decades and have

64   provided a large amount of atmospheric Hg data. Compared to Europe and the United States,

Atmospheric
Chemistry
and Physics
Discussions

65 independent research teams have conducted monitoring work in China based on different research

66 interests (Fu et al., 2012b;Fu et al., 2008;Fu et al., 2016a;Fu et al., 2019;Fu et al., 2016b;Liu et al.,

67 2011;Feng and Fu, 2016;Feng et al., 2013;Wang et al., 2015;Hu et al., 2014;Ci et al., 2011;Duan et

68 al., 2017;Liu et al., 2002;Yin et al., 2018;Yin et al., 2020b;Lin et al., 2022;Lin et al., 2019). Most

69 monitoring stations are set up only in developed regions, such as eastern and central China, owing

70 to operational difficulties in remote areas. Few studies on atmospheric Hg in western China have

71 been reported; thus, little is known about the overall level of atmospheric Hg in western China. To

72 better employ the Minamata Convention and verify the effect of the implementation of the

73 Convention, monitoring atmospheric Hg concentrations around the globe is significant and can aid

74 in identifying the global Hg transport pattern.

75 The Tibetan Plateau is in the mid-latitudes of the Northern Hemisphere (in central Asia) and is

76 an important area for studying the global Hg circulation. Owing to the high altitude and rough living

77 conditions, there is little Hg research on the Tibetan Plateau. This area is less developed and there

78 are few industrial activities; therefore, it is generally considered a clean region and can be treated

79 as a background condition. However, there are large tourist cities in this area, such as Lhasa, where

80 the number of tourists reached 40,121,522 in 2019 (Tibet Bureau of Statistics, 2020). Local cement

81 production in Tibet reached 10.81 million tons in 2019 (Tibet Bureau of Statistics, 2020).

82 Meanwhile, although the high altitude makes the Tibetan region a natural barrier between inland

83 China and the Indian subcontinent (Qiu, 2008;Yao et al., 2012;Pant et al., 2018), the Tibetan Plateau

84 is potentially influenced by the Indian summer monsoon (ISM) and the Westerly circulation (WEC).

85 Trans-boundary inputs of atmospheric pollutants to the Tibetan Plateau have been demonstrated in

86 pollutant studies such as with persistent organic pollutants and black carbon (Yang et al., 2018;Li et

87 al., 2016a;Zhang et al., 2015b;Pokhrel et al., 2016;Wang et al., 2018;Zhang et al., 2015a;Feng et al.,

88 2019;Zhu et al., 2019). Our previous study on atmospheric Hg in the Qomolangma region (QNNP)

89 also suggested that atmospheric Hg from India can be transported and affect atmospheric Hg

90 concentrations on the Tibetan Plateau as a result of the Indian monsoon (Lin et al., 2019). Hence, it

91 remains unclear whether the Tibetan Plateau can be treated as a background area for studying

92 atmospheric Hg, and further monitoring data are required. Monitoring in the largest cities on the

93 Tibetan Plateau will provide important information and corroboration to address this query.

94   In previous study, Yin et al. (2018) reported GEM concentration data for the Namco region on

95 the Tibetan Plateau from 2012-2014 and found that the GEM concentration at Namco was $1.33 \pm$

96 0.24 ng m^{-3}, which is lower than the mean GEM concentration in the Northern Hemisphere

97 (Lindberg et al., 2007;Slemr et al., 2015;Venter et al., 2015;Sprovieri et al., 2016;Lan et al., 2012).

98 Our previous study at QNNP (Lin et al., 2019) showed that the atmospheric Hg concentrations were

99 1.42 ± 0.37 ng m^{-3}, 21.4 ± 13.4 pg m^{-3}, and 25.6 ± 19.1 pg m^{-3} for GEM, GOM, and PBM,

100 respectively, close similar to the average GEM concentrations in the Northern Hemisphere. The

101 concentrations of atmospheric Hg species in Nyingchi, in the southeast Tibetan Plateau, were very

102 low (1.01 ± 0.27 ng m^{-3}, 12.8 ± 13.3 pg m^{-3}, and 9.3 ± 5.9 pg m^{-3} for GEM, GOM, and PBM,

103 respectively), which may be affected by heavy wet deposition and the large amounts of vegetation

104 in the Yarlung Zangbu/Brahmaputra Grand Canyon (Lin et al., 2022). However, Namco, QNNP

105 and Nyingchi are remote areas on the Plateau, with few populations and industries. During previous

106 studies in Lhasa, the largest city on the Plateau, only dry and wet depositions of atmospheric Hg

107 were analyzed. Monitoring of atmospheric Hg particulate matter (Huang et al., 2016a) indicated that

108 Lhasa has mean particulate Hg levels as high as 224 pg m^{-3} (ranging from 61.2 to 831 pg m^{-3}),

109 which is much higher than expected. Huang et al. (2013) measured the wet deposition of

110 atmospheric Hg in Lhasa in 2010 and showed that the wet deposition of total Hg and particulate Hg

111 was higher during the non-monsoon period than during the monsoon period. The active Hg was

112 higher during the monsoon than during the non-monsoon period, and they concluded that the wet

113 deposition of Hg originated mainly from local sources. This indicates that atmospheric Hg

114 concentrations in Lhasa may be elevated and further detailed monitoring is needed.

115   In this study, we conducted a high-time-precision atmospheric Hg species monitoring system

116 in Lhasa. We performed cont inuous measurements of GEM, GOM, and PBM concentrations from

117 subsequent of the Indian Summer Monsoon (S-ISM) period to the WEC period from 2016 to 2017.

118 Based on literature research, this is the first continuous monitoring of atmospheric Hg species in a

119 city on the Tibetan Plateau, and the influence of human activities, meteorological factors, and long-

120 range transportation of pollutants on the diurnal variation of atmospheric Hg in Lhasa is discussed.

121 We combined monitoring with other pollutant concentrations to explore the main factors influencing

122 the local atmospheric Hg concentrations. To determine the detailed source profile of atmospheric

123   Hg, we combined real-time Hg monitoring data with backward trajectory and cluster analyses. This

124   study can help understand atmospheric Hg characteristics in the city of the Plateau and provide

125   scientific support for managerial decision-making.

126   **2.   Material and methods**

127   **2.1   Atmospheric Hg monitoring sites**

128   The monitoring site for atmospheric Hg species in Lhasa was set up on the top floor of the

129   Lhasa station office building in the Institute of Tibetan Plateau Research, Chinese Academy of

130   Sciences, in western Lhasa City (29.64°N, 91.03°E, 3650 m above sea level; Figure 1, Figure S1).

131   Lhasa is located in the central region and is the largest city on the Tibetan Plateau, covering an area

132   of approximately 60 km^2. The Lhasa population in 2019 was 720,700, accounting for approximately

133   20.6% of the total population of the Tibet Autonomous Region (Tibet Bureau of Statistics, 2020).

134   The entire city is in a flat river valley surrounded by mountains up to 5,500 m above sea level.

135   During the ISM period (from May to September), the low pressure on the Tibetan Plateau attracts

136   the summer monsoon from the Indian Ocean to the Plateau, exhibiting a wetter monsoon season

137   (Qiu, 2008). During the non-monsoon season (from October to April), the large-scale atmospheric

138   circulation on the Tibetan Plateau is mainly under the control of westerly winds, which largely come

139   from the inland areas of Central Asia, presenting a drier season in Lhasa during this time (Huang et

140   al., 2010;Guo et al., 2015). According to previous studies, the air quality in Lhasa may be influenced

141   by local emissions from anthropogenic activities (e.g., power plants, cement facilities, vehicular

142   traffic, and religious activities) (Li et al., 2008;Cong et al., 2011;Huang et al., 2010;Guo et al.,

143   2015;Luo et al., 2016;Li et al., 2016b) and long-range transboundary atmospheric transport (Huang

144   et al., 2016a;Huang et al., 2016b).

Atmospheric
Chemistry
and Physics
Discussions
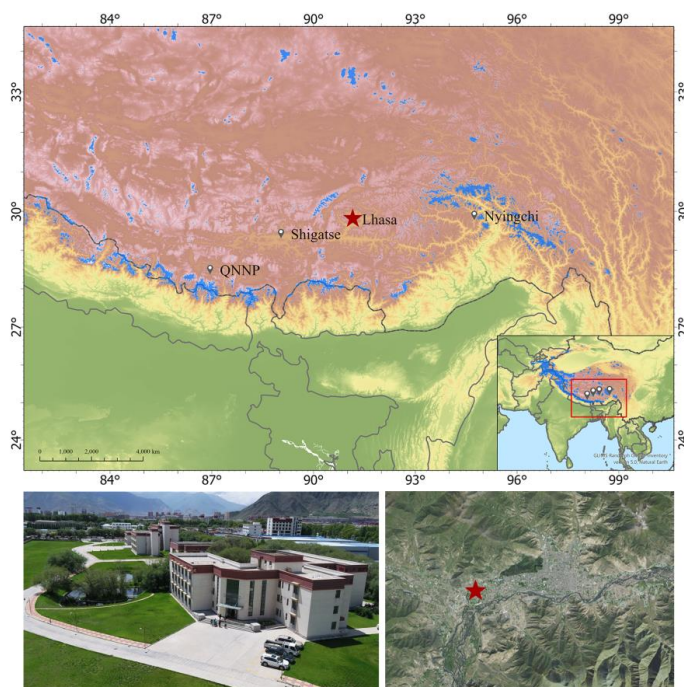
Figure 1 Location of the Lhasa station in the Institute of Tibetan Plateau Research,

Chinese Academy of Sciences (red star).

2.2 GEM, GOM, and PBM active monitoring

Monitoring in Lhasa was performed using Tekran models 2537 B, 1130, and 1135 (Tekran Inc., Toronto, Canada) for real-time continuous measurements of GEM, GOM, and PBM concentrations. Model 2357b is the main analytical module used to analyze Hg concentrations employing the cold atomic fluorescence technique. Model 1130 is divided into pump and lysimeter modules, which is mainly used for the collection and resolution of GOM. Model 1135 is the particle collection module that is mainly used to collect and analyze atmospheric Hg in the particulate state. During the actual monitoring, considering the low air pressure on the Tibetan Plateau, we reduced the airflow of the pump module to 7.5 L/min (Swartzendruber et al., 2009;Zhang et al., 2015a;Zhang et al., 2016;Lin et al., 2019;Lin et al., 2022) and the airflow in model 2537B was reduced to 1 L/min to ensure that atmospheric Hg monitoring could be continuously performed. All monitoring data were converted to concentrations under standard atmospheric pressure. The Tekran 2537B analyzer was

161   automatically calibrated every 23 hours using the instrument's internal Hg permeation source and

162   was calibrated before and after monitoring using an external Hg source. The same instrument setup

163   was used for QNNP and Nyingchi (Lin et al., 2019;Lin et al., 2022). The Tekran ambient Hg

164   analyzer has been described in detail in previous studies (Landis et al., 2002; Rutter et al. 2008; de

165   Foy et al. 2016).

2.3   Meteorological data and other pollutant data

167   During the monitoring period, the Vantage Pro2 weather station (Davis Instruments, USA)

168   recorded local temperature (accuracy of 0.1°C), relative humidity (accuracy of 1%), wind speed

169   (accuracy of 0.1 m s^{-1}), wind direction (accuracy of 1°), barometric pressure (accuracy of 0.1 hPa),

170   solar radiation (accuracy of 1 W m^{-2}), and UV index (accuracy 0.1 MEDs). Hourly measurements

171   of $PM_{2.5}$, PM_{10}, SO_2, NO_2, O_3, and CO concentrations and the air quality index (AQI) were obtained

172   from monitoring stations hosted by the Ministry of Ecology and Environment of China and

173   published by the China Environmental Monitoring Center. The station was set up 10 km from the

174   atmospheric Hg monitoring station.

2.4   Backward trajectory simulation and potential source analysis

176   To better understand the transport paths of atmospheric GEM, the Hybrid Single-Particle

177   Lagrangian Integrated Trajectory (HYSPLIT) model was used to calculate backward trajectories

178   (Stein et al., 2015;Chai et al., 2017;Chai et al., 2016;Hurst and Davis, 2017;Lin et al., 2019). The

179   HYSPLIT model (https://www.arl.noaa.gov/hysplit/hysplit/) is a hybrid approach that combines

180   Lagrangian and Eulerian methods, which was developed by the National Oceanic and Atmospheric

181   Administration (NOAA) as a tool to explain the transport, dispersion, and deposition of particles in

182   the atmosphere. The backward trajectory simulation used Global Data Assimilation System (GDAS)

183   data with 1°x1° latitude and longitude horizontal spatial resolution and 23 vertical heights every 6

184   hours in this study. We examined the effect of arrival height on the trajectories using different arrival

185   heights (50 m, 100 m, 400 m, and 1,000 m) in December 2016 (Figure S2). The results showed that

186   the calculated trajectories of the air masses were almost the same when the arrival height was below

187   400 m. The trajectory arrival altitude was then set to 100 m a.g.l in this study. The trajectories were

188   computed every 6 hours with an inverse time of 120 hours. The trajectories could cover China,

189   Nepal, India, Pakistan, and most of West Asia. Here, we combined the backward trajectory with

190   real-time Hg monitoring concentrations to represent the trajectories of GEM concentrations. Cluster

191   analysis was performed after the trajectory calculation. Cluster analysis can indicate the main

192   trajectory of incoming pathways and the GEM concentration indicated by the incoming trajectories.

193   **2.5 Principal component analysis**

194   Principal component analysis (PCA) is a data reduction method that allows a number of

195   measured variables to be catergorized into several factors that represent the behavior of the entire

196   dataset (Jackson, 2005). In many previous Hg studies, PCA has been used to analyze the

197   relationships between Hg and multiple pollutants and meteorological variables (Brooks et al.,

198   2010;Cheng et al., 2012;Liu et al., 2007;Zhou et al., 2019;Lin et al., 2022). Prior to running the

199   PCA, all variables were normalized by the standard deviation. To check whether PCA was the

200   appropriate method for the dataset used in this study, Kaiser-Meyer-Olkin's measure of sampling

201   adequacy (MSA>0.5) and Bartlett's Test of sphericity (P<0.05) tests were performed during data

202   analysis. Total variance and rotated scree plots were used to determine the number of factors during

203   the PCA analysis, and components with variance ≥ 1.0 were retained. Variables with high factor

204   loadings (generally >0.5) were identified as potential sources of Hg in this study.

205   **3.   Results and Discussion**

206   **3.1   Atmospheric Hg Monitoring in Lhasa**

207   Atmospheric Hg monitoring in Lhasa comprised the subsequent Indian Summer Monsoon (S-

208   ISM) and Westerly circulation (WEC) periods. Figure 2 shows the variation in atmospheric Hg

209   concentrations at the station during the monitoring period. During the whole monitoring period, the

210   mean concentrations of GEM, GOM, and PBM at the station were 2.26 ± 1.97 ng m^{-3}, 36.4 ± 48.9 pg

211   m^{-3}, and 54.5 ± 119.5 pg m^{-3} (mean concentration $\pm$ standard deviation), respectively. During the S-

212   ISM period, the concentrations of GEM, GOM, and PBM were 2.73 ± 1.48 ng m^{-3}, 38.4 ± 62.7 pg m^{-}

213   ^{3}, and 59.1 ± 181.0 pg m^{-3}, respectively, while during the WEC period, the concentrations of GEM,

214   GOM, and PBM were 2.11 ± 2.09 ng m^{-3}, 35.8 ± 43.3 pg m^{-3}, and 52.9 ± 90.1 pg m^{-3}, respectively. The

215   GEM concentrations during the S-ISM period were significantly higher than those during the WEC

216   period ($p < 0.01$), while the mean concentrations of GOM and PBM in the S-ISM period were

217   slightly higher than those in the WEC period. Overall, GEM concentrations showed a decreasing

218   trend throughout the monitoring period, with the average weekly concentration decreasing from

219 3.21 ng m^{-3} at the beginning of the monitoring period to 1.60 ng m^{-3} at the end of the monitoring

220 period. Unexpectedly high concentrations were found at irregular intervals for all Hg species. The

221 occurrence time of these high concentrations was random, and high GEM concentrations did not

222 always occur at the same time as high GOM or PBM concentrations, indicating the complexity of

223 the Hg sources of the species. For GOM and PBM, relatively comparable trends between them may

224 be related to similar sources, transport, and transformation reactions in the atmosphere.
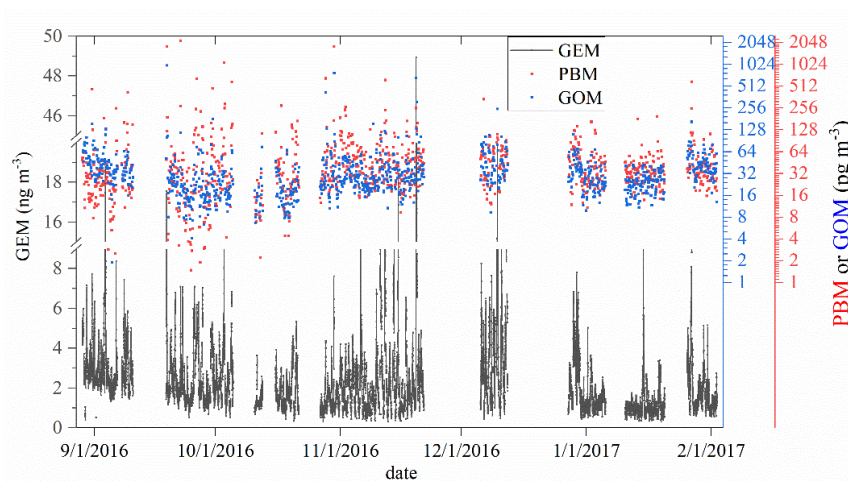
225

226 **Figure 2 Time series of GEM, GOM, and PBM concentrations over the sampling period. The**

227 **GEM concentration resolution was 5 min and the GOM and PBM resolutions was 2 h.**

228

229   In early September, GOM concentrations were generally higher than PBM concentrations. In

230 the subsequent period, PBM concentrations were always higher than GOM concentrations, which

231 may indicate that the sources and composition of pollutants at this time were not consistent with

232 those in the latter period. The GOM and PBM concentrations were higher in November and

233 December. Since GOM and PBM are mainly from local emissions, the changes in their

234 concentrations may indicate that there are more local sources at this period. As Lhasa enters the

235 heating season in November-December, and there are more local religious activities at this time,

236 there may be more local combustion sources. Table 1 lists the concentrations of Hg and other

237 pollutants during the monitoring period. PM$_{2.5}$ concentration increased significantly in the WEC1

238 period, indicating the presence of more particulate matter during this period. This could explain the

Atmospheric
Chemistry
and Physics
Discussions

239   elevated concentrations of GOM and PBM from November-December.

Table 1 Statistics metrics of species Hg, meteorological factors, and other pollutants

Period	Stat	GEM (ng m^{-3})	PBM (pg m^{-3})	GOM (pg m^{-3})	Temp (°C)	Hum. (%)	Wind speed (m s^{-1})	Solar radiation (W m^{-2})	CO (mg m^{-3})	NO$_2$ (μg m^{-3})	O$_3$ (μg m^{-3})	PM$_{2.5}$ (μg m^{-3})	SO$_2$ (μg m^{-3})
S-ISM	Mean	2.73	59.08	38.39	14.42	61.45	1.70	212.60	0.39	26.44	72.18	16.26	4.19
	SD	1.48	181.38	62.85	3.70	16.96	1.41	313.90	0.18	19.36	28.68	13.12	2.08
	Median	2.36	24.50	30.30	13.90	62.00	1.30	7.00	0.30	22.00	77.00	13.00	4.00
	Min	0.40	-11.44	1.89	5.90	14.00	0.00	0.00	0.10	1.00	1.00	1.00	1.00
	Max	18.87	2165.70	988.50	24.70	93.00	13.00	1290.00	1.70	110.00	133.00	81.00	21.00
WEC1	Mean	2.39	57.55	37.46	6.90	26.01	1.28	169.56	0.64	45.24	45.39	47.97	5.51
	SD	2.35	104.15	50.98	5.75	15.08	1.39	246.66	0.51	31.01	34.44	46.19	5.35
	Median	1.79	38.80	27.83	6.90	24.00	0.90	0.00	0.50	41.00	43.00	35.00	5.00
	Min	0.31	0.00	1.89	-6.20	1.00	0.00	0.00	0.10	2.00	1.00	1.00	1.00
	Max	48.93	1797.30	774.86	21.60	94.00	9.80	973.00	4.40	152.00	133.00	458.00	145.00
WEC2	Mean	1.47	42.82	32.05	0.22	25.59	1.97	123.61	0.56	26.78	65.22	23.73	4.49
	SD	1.12	45.39	17.14	3.98	14.67	1.85	186.98	0.30	22.61	26.30	18.77	2.61
	Median	1.17	33.77	27.50	0.20	24.00	1.30	0.00	0.50	19.00	71.00	19.00	4.00
	Min	0.33	0.00	9.91	-8.80	2.00	0.00	0.00	0.20	2.00	1.00	1.00	1.00
	Max	20.86	589.43	165.06	10.20	68.00	11.20	662.00	2.60	99.00	108.00	118.00	32.00

240

241   Table 2 shows the distributions of atmospheric Hg concentrations in some provincial capitals

242   in China and nearby monitoring stations from literature. In general, the GEM concentration in Lhasa

243   is low among the provincial capitals in China. The GEM concentration in other provincial capitals

244   of China was approximately 3-10 ng m^{-3}. Guiyang, Chongqing, and Lanzhou were the nearest

10

Atmospheric
Chemistry
and Physics
Discussions
Open Access
EGU

245   provincial capitals to Lhasa, with GEM concentrations reported in the literature, all located in

246   western China. Guiyang had a very high GEM concentration due to the presence of local Hg mines

247   (Liu et al., 2011;Yang et al., 2009). The GEM concentration in Chongqing was approximately three

248   times higher than that of Lhasa. The higher GEM concentration in Chongqing was likely due to its

249   proximity to the Hg-contaminated area and large population (Yang et al., 2009). Compared to

250   Lanzhou, another high-altitude city, the GEM concentration in Lhasa was approximately half that

251   of Lanzhou, which may be owing to the overall cleaner environment with fewer local pollution

252   sources in Lhasa (Yin et al., 2020a). The GOM and PBM concentrations in other provincial capitals

253   were relatively less monitored. However, GOM concentrations in Lhasa were significantly higher

254   than those in cities with GOM monitoring, such as mega-cities like Beijing and Shanghai, and even

255   higher than those in Guiyang, where Hg mines are located. GOM concentrations in provincial

256   capitals nationwide were mainly concentrated between 3-20 pg m^{-3}, whereas the GOM

257   concentrations in Lhasa were approximately 2-10 times higher than the average concentration in

258   provincial capitals. The high GOM concentration in Lhasa is likely due to its high altitude. Lhasa is

259   exposed to much higher solar radiation and has more ice surfaces than inland areas, which may have

260   contributed to the oxidation of GEM or the re-release of GOM deposited in snow and ice (Steffen

261   et al., 2008;Dommergue et al., 2003;Song et al., 2018). In contrast, the PBM concentration in Lhasa

262   was at a lower level, only somewhat higher than that in Hefei. The monitoring period in Lhasa was

263   mainly in winter when there were more particulate matter emissions than in summer owing to

264   heating combustion. The PM$_{2.5}$ concentration in Lhasa was low throughout the monitoring period

265   (Table 1), which indicated that the local particulate matter emissions were low; this may be the main

266   reason for the low PBM concentration.

Atmospheric Chemistry and Physics

Discussions

267

Table 2 Comparison of atmospheric Hg concentrations at some provincial capitals in China and some nearby monitoring stations

location	altitude	type	region	Monitoring period	GEM (ng m⁻³)	GOM (pg m⁻³)	PBM (pg m⁻³)	GEM diurnal variation (local time) peak	valley	variation	reference
Lhasa	**3600**	**City**	**Southwest**	**8/2016-2/2017**	**2.26±1.97**	**36.4±48.9**	**54.5±119.5**				**This study**
Beijing	40	City	North china	12/2008-11/2009	3.22±1.74	10.1±18.8	98.2±112.7				(Zhang et al., 2013)
Hefei	30	City	East china	7/2013-6/2014	4.07±1.91	3.67±5.11	30.0±100.3				(Hong et al., 2016)
Shanghai	4	City	East china	2014	4.19±9.13	21±100	197±877				(Duan et al., 2017)
Lanzhou	1525	City	Northwest	10/2016-10/2017	4.48±2.32	-	-				(Yin et al., 2020a)
Jinan	148	City	East china	10/2015 -7/2016	4.91±3.66	-	451.9±433.4				(Li et al., 2017)
Chongqing	300	City	Southwest	2006-2007	6.74±0.37	-	-				(Yang et al., 2009)
Nanjing	25	City	East china	2011	7.9±7.0	-	-				(Zhu et al., 2012)
Guiyang	1150	City	Southwest	8/2009-12/2009	9.72±10.2	35.7±43.9	368±676				(Liu et al., 2011)
Ev-K2, Nepal	5050	Remote		11/2011-4/2012	1.2±0.2	-	-	18/1.30	6/1.10	0.20	(Gratz et al., 2013)
Nam Co, China	5300	Remote		11/2014-3/2015	1.33±0.24	-	-	-	-	-	(Yin et al., 2018)
Waliguan, China	3816	Remote		9/2007-9/2008	1.98±0.98	7.4±4.8	19.4±18.1	6/2.30	14/1.94	0.36	(Fu et al., 2012a)
Shangri-La, China	3580	Remote		11/2009-11/2010	2.51±0.73	8.22±7.9	38.32±31.26	17/2.48	6/1.71	0.77	(Zhang et al., 2015a)
Gongga, China	1640	Remote		5/2005-6/2006	3.98	-	-	11/4.45	2/3.55	0.90	(Fu et al., 2008)
QNNP, China	4267	Remote		4/2016-8/2016	1.42±0.37	21.4±13.4	25.6±19.1	6/2.04	13/1.11	0.93	(Lin et al., 2019)
Nyingchi, China	3263	Remote		3/2019-9/2019	1.01±0.27	12.8±13.3	9.3±5.9	20/1.07	6/0.96	0.11	

268   Compared to nearby monitoring stations (Table 2), Hg species concentrations in Lhasa were

269   high. Namco station is the nearest station; its altitude is 4,730 m and the distance between the two

270   stations is approximately 120 km. The GEM concentration in Namco was 1.33 ± 0.24 ng m^{-3}, which

271   was only 59% of Lhasa. This is likely because the Namco region is sparsely populated with minimal

272   local pollution and is far from major Hg pollution sources (Yin et al., 2018). Compared to the QNNP

273   (Lin et al., 2019) on Mt. Everest, which is approximately 500 km apart, the GEM, GOM, and PBM

274   concentrations in Lhasa were approximately 1.6, 1.7, and 2.1 times higher, respectively. Our

275   previous studies demonstrated that the QNNP is influenced by transported air masses from the

276   Indian subcontinent, indicating that the concentration in Lhasa is high in the Tibetan Plateau.

277   Compared to another typical highland site, Nyingchi, Lhasa had much high levels of atmospheric

278   Hg species, which may be related to the vegetation uptake effects and strong wet deposition in

279   Nyingchi (Lin et al., 2022). Among the surrounding stations, only Mt. Gongga and Shangri-La

280   stations had higher GEM concentrations than Lhasa. The GEM concentrations reported at Mt.

281   Gongga station ranged from May 2005 to July 2006. Considering that the smelting activities near

282   this site were crude at that time and there were almost no air pollution control measures, the high

283   local GEM concentrations may be strongly affected by local smelting activities and fuel combustion

284   (Fu et al., 2008). In contrast, GEM concentrations in the Shangri-La region were mainly controlled

285   by the monsoon, and Zhang et al. (2015a) suggested that all local GEM above 2.5 ng m^{-3} are

286   associated with the transport of dry air carrying domestic and foreign regional anthropogenic

287   emissions. Comparing these sites only for the monsoon period, the GEM concentration in Lhasa

288   was higher than that in the Shangri-La region. As for GOM and PBM, the concentrations at the

289   Lhasa station were much higher than those in the surrounding areas. The average GOM

290   concentration in the surrounding areas was approximately 10 pg m^{-3}, which was only 27% of that

291   in Lhasa, and the average PBM concentration in the surrounding areas was approximately 28 pg m^{-}

292   ^{3}, which was only 54% of that in Lhasa. Considering that GOM and PBM are mainly from local or

293   surrounding sources or atmospheric transport (Lindberg and Stratton, 1998;Seigneur et al.,

294   2006;Lynam et al., 2014), high GOM and PBM concentrations may indicate additional local sources

295   of Hg in Lhasa.

296   **3.2   Unexpected high concentration events in Lhasa**

297   To investigate the reasons for the random high atmospheric Hg concentration events in Lhasa,

298   typical high-value occurrence processes (defined as GEM concentrations above 10 ng m^{-3} monitored

299   more than five times on a single day) were selected for analysis in the S-ISM and WEC periods,

300   respectively. A total of seven high GEM concentration events were identified, of which, September

301   3, November 10, November 19, and December 9, 2016, were selected for analysis; September 18,

302   October 3, 2016, and January 27, 2017 were omitted due to lack of meteorological data or Hg

303   concentration data for the proximity date.

304   During the S-ISM period (Figure 2), there was a clear peak in Hg concentration on September

305   3, while the GEM, GOM, and PBM concentrations were approximately 1.6, 1.5, and 2.3 times the

306   average daily value, respectively. Comparing the two days before and after the high-concentration

307   event (Table 3, Figure 3. a), the concentrations of the three pollutants NO$_2$/PM$_{2.5}$/SO$_2$, were higher

308   on September 3. High GEM concentrations were accompanied by winds of 2.12 m/s from the

309   southwest, with NO$_2$ and SO$_2$ concentrations higher than usual as well as increased PBM

310   concentrations. NO$_2$ and SO$_2$ are typical combustion source pollutants, and the presence of PM$_{2.5}$,

311   and PBM may indicate more combustion sources in the day. Thus, it can be inferred that the elevated

312   Hg concentration event on September 3 may have originated mainly from a combustion event

313   nearby or further away.

314   During the WEC period, significantly high values were observed on November 10, November

315   19, and December 9. On November 10 (Figure 3.b), the increase in atmospheric Hg species

316   concentrations was accompanied by significant increases in CO/NO$_2$/PM$_{10}$/PM$_{2.5}$/SO$_2$

317   concentrations. Two similar peaks in atmospheric Hg species concentrations were also observed

318   around November 10, with relatively lower peak concentrations. During these three events, the

319   concentrations of other pollutants were higher than usual, whereas wind speeds were extremely low

320   during the event periods. In addition, extremely high PBM concentrations (297.7±189.3 pg m^{-3},

321   maximum 621.2 pg m^{-3}) were observed at midnight on November 12 which, considering the

322   extremely low wind speed and the presence of a low height nocturnal boundary layer, may indicate

323   that the high concentrations originated from local sources.

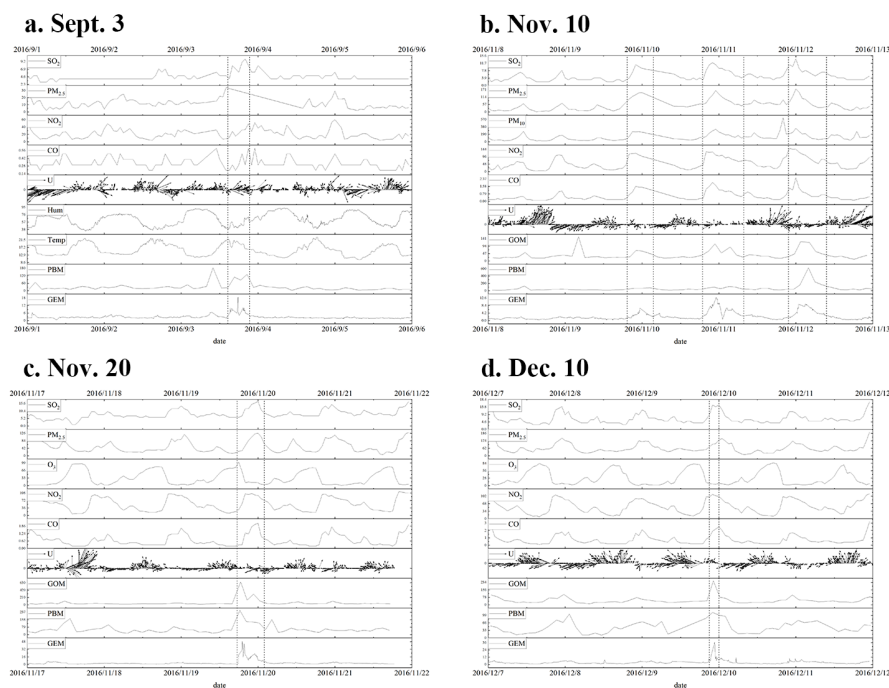Table 3 Comparation of the pollutant concentrations with the two days before and after the high Hg concentration events

Item		9.1-2	9.3	9.4-5	11.8-9	11.10	11.11-12	11.17-18	11.19	11.20-21	12.7-8	12.9	12.10-11
GEM	(ng m^{-3})	2.72	4.63	3.03	1.47	3.16	2.96	2.15	6.87	2.66	2.76	5.43	3.24
PBM	(pg m^{-3})	25.32	64.17	31.52	36.31	47.21	94.80	53.41	74.78	55.40	38.71	66.74	49.05
GOM	(pg m^{-3})	40.95	63.84	42.55	32.76	39.48	42.03	35.29	119.39	44.86	43.84	69.65	43.75
Temp.	(°C)	16.61	15.86	15.32	7.06	7.76	8.80	4.20	4.49	4.94	3.13	2.88	2.77
Hum.	(%)	58.47	67.89	68.71	19.96	22.02	21.04	21.82	23.35	25.67	23.50	26.86	26.09
Wind	(m s^{-1})	2.37	1.46	1.49	1.47	0.93	1.17	1.05	0.71	0.75	0.88	0.89	0.67
Barometer	(hPa)	651.62	651.08	652.39	654.90	654.33	652.31	655.11	652.18	653.57	657.99	655.66	653.08
rainfall	(mm)	0.01	0.17	0.36	0.00	0.00	0.00	0.00	0.00	0.00	0.00	0.00	0.00
Solar Rad.	(W m^{-2})	241.20	201.15	214.39	189.02	194.45	182.30	166.14	161.59	180.02	141.61	139.69	136.64
CO	(mg m^{-3})	0.34	0.36	0.32	0.39	0.76	0.63	0.64	0.71	0.72	0.67	0.80	0.74
NO$_2$	(µg m^{-3})	20.44	26.00	21.77	41.38	57.64	66.48	54.58	53.58	55.27	48.87	55.33	56.23
O$_3$	(µg m^{-3})	85.73	77.42	72.56	59.27	57.43	49.46	34.73	34.79	29.51	31.37	28.38	26.81
PM$_{10}$	(µg m^{-3})	33.90	32.78	26.95	80.71	130.07	155.44	107.98	119.79	146.29	125.82	137.74	143.13
PM$_{2.5}$	(µg m^{-3})	11.98	17.10	10.98	31.20	75.07	64.85	51.21	50.13	53.83	62.80	65.46	62.71
SO$_2$	(µg m^{-3})	4.23	5.89	4.91	3.83	6.07	5.71	6.50	8.92	9.44	6.00	6.88	6.69

324

325   On November 19 (Figure 3.c), there was a significant increase in all atmospheric Hg species

326   concentrations. During the elevated period, the average GEM, GOM, and PBM concentrations were

327   17.94±10.54 ng m^{-3}, 302.5±218.5 pg m^{-3}, and 162.4±54.0 pg m^{-3}, respectively, which were 8.3, 5.7,

328 and 4.6 times higher than the average concentrations on November 17-18. However, only a slight

329 increase in the peak CO/ $PM_{2.5}$/SO_2 concentration was observed during the event period. Therefore,

330 the increase in atmospheric Hg species concentrations may indicate that this event was unique, with

331 certain sources of high Hg concentrations. The low wind speed and low nocturnal boundary layer

332 height both contributed to the accumulation of atmospheric Hg species, which also indicated that

333 the elevated Hg was from local sources. Similar to the event on November 19, sharp increases in

334 atmospheric Hg species concentrations were observed only on December 9 (Figure 3.d). The

335 atmospheric Hg species concentration increase events during the WEC period occurred at night and,

336 given that it coincided with the winter heating period, local combustion sources may be the unique

337 sources that may contribute to the Hg concentration increase.

338

Figure 3 Comparison of the pollutant concentrations with the two days before and after the

high Hg concentration events

3.3 Diurnal variation of atmospheric Hg in Lhasa

342 Figure 4.a shows the diurnal variation of atmospheric Hg in Lhasa during the monitoring period.

343 The mean GEM concentration during this period was 2.26±1.97 ng m^{-3}, and the maximum

344   difference of hourly average GEM diurnal variation was 1.89 ng m^{-3}. GEM concentration was low

345   during the day; the lowest concentration of the day appeared from 14:00-18:00 (UTC+8). The GEM

346   concentration kept increasing and reached the peak at midnight. During the night, the GEM

347   concentration maintained in high value with little dissipation. Subsequently, the GEM concentration

348   decreased rapidly with the sunrise. Overall, the diurnal variation of GEM concentration was similar

349   to CO, NO$_2$, and relative humidity, and opposite to O$_3$ and wind speed. The high GEM

350   concentrations at night can be attributed to the lower boundary layer height at night (average at 131

351   m a.g.l. during the observation period, between 19:00 and 07:00, UTC+8) and the lower wind speed

352   (Figure 4). Also, the average night temperature in Lhasa during the monitoring period was 5.8℃,

353   and the residents heating combustion may bring about the release of GEM. After sunrise, the

354   boundary layer height increased rapidly and the diffusion quickly occurred in the lower atmosphere.

355   During the increase of wind speed, airflows were carried from other regions with few populations,

356   which may lead to a decrease in GEM concentrations. For both GOM and PBM, the higher GOM

357   concentrations occurred during the day and higher PBM concentration occurred during the night.

358   No obvious increase occurred for GOM and PBM concentrations at the same time, which may

359   indicate that there is no local common external source, and the variation of GOM and PBM

360   concentrations may come from the gas-particle redistribution process of atmospheric Hg(II).
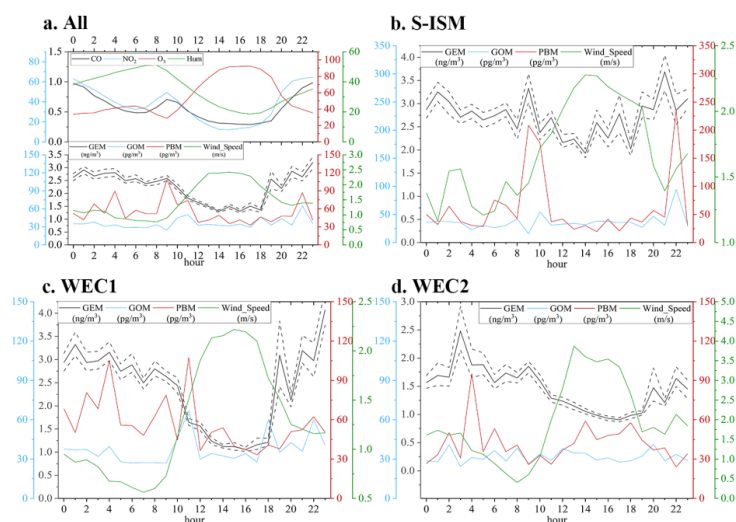
361

362   **Figure 4 Diurnal variations of Hg species, concentrations of other pollutants, and**

363   **meteorological information from S-ISM to WEC periods. The short horizontal line**

Atmospheric
Chemistry
and Physics
Discussions

Open Access
EGU

364   **represents the concentration error range for each time period.**

365   In particular, during the S-ISM period (Figure 4.b), the diurnal variation in GEM

366   concentrations fluctuated frequently, which indicates that the factors affecting the concentration

367   variation were very complicated. The mean concentration of GEM during this period was 2.73 ng

368   m^{-3}, and the maximum difference of GEM diurnal variation was 1.40 ng m^{-3}. September was the

369   ending period of the Indian summer monsoon, and the external transboundary transport of air masses

370   by the monsoon may have been weakened. Simultaneously, the average temperature in September

371   was high (14.4°C) without residents heating during the night, which may be the reason for the small

372   diurnal variation in GEM concentrations. Overall, GEM concentrations remained lower during the

373   day, increased, and remained high at night. No clear pattern of variation was observed in GOM and

374   PBM during this period.

375   During the WEC1 period, the diurnal variation in GEM concentrations was exceedingly large.

376   The mean GEM value was 2.39 ng m^{-3} with great GEM diurnal variation value (3.01 ng m^{-3}). The

377   diurnal trend was roughly the same as the whole monitoring period, but the lowest value was 1.06

378   ng m^{-3} and the highest value was 4.07 ng m^{-3}. The increase in night concentrations may be related

379   to the beginning of the heating season, whereas the burning of yak dung, firewood, or other fuels

380   for residential heating may release GEM and PBM, and accumulate within the boundary layer at

381   night, leading to higher GEM concentrations (Rhode et al., 2007;Xiao et al., 2015;Chen et al., 2015).

382   In contrast, low day values may be related to the wind field. Although the wind speed during the

383   WEC1 period was similar to that during the S-ISM period, westerly circulation was prevalent in

384   Lhasa during the WEC1 period, with air masses coming from the sparsely populated area with lower

385   GEM concentrations. The westerly winds carry away the locally accumulated GEM air masses in

386   Lhasa and bring in low GEM concentration air masses from west of Lhasa. During this period, the

387   diurnal variation in GOM concentrations was not clear.

388   The influence of wind flow was evident during the WEC2 period. During this period, GEM

389   concentrations in Lhasa were the lowest and close to 1.00 ng m^{-3} in the late afternoon when wind

390   speeds were the highest. Nighttime concentrations were lower in the WEC2 period than in the

391   WEC1 period, probably because wind speeds were also high at night during the WEC2 period

392   (19:00-4:00 UTC+8, mean wind speed 1.74 m/s). The heating season was still in progress during

Atmospheric
Chemistry
and Physics
Discussions
Open Access
EGU

393   the WEC2 period, but GEM emissions from heating were likely carried away by the continuous

394   flow of air masses. Therefore, the mean GEM concentration in Lhasa during the winter was likely

395   strongly influenced by wind speed.

396   Compared to the diurnal variation patterns obtained from monitoring in other remote areas of

397   China (Figure S3), the diurnal variation of GEM in Lhasa is more unique, and a wide diurnal

398   variation in concentration was observed. Valleys of GEM concentrations in the afternoon were also

399   observed in Waliguan and Namco, but the concentration variation ranges were small in both areas.

400   This could be related to the regional characteristics of the three sites. Waliguan is located in a

401   mountainous area with no significant local anthropogenic sources, and is mainly influenced by

402   valley winds (Fu et al., 2012a). Namco is located in the central Tibetan region away from

403   anthropogenic sources. Although the wind speed was also high in the afternoon in Namco (Yin et

404   al., 2018), it is likely that the diurnal variation in atmospheric GEM concentrations was small

405   because the atmosphere was well-proportioned and there were no local sources; therefore, the

406   changes in wind speed might not affect the GEM concentration. In contrast, with the difference in

407   GEM concentrations between Lhasa and the transmitted external air mass, wind speed could

408   significantly influence the GEM concentrations in Lhasa. Meteorological conditions may have

409   played a more important role. We conjecture that the high nighttime concentrations in Lhasa may

410   originate mainly from local emissions, while the high wind speed and mixing of clean external air

411   masses in the afternoon reduce the local GEM concentrations.

412   **3.4   Analysis of factors affecting atmospheric Hg concentration in Lhasa**

413   Overall, four components were resolved for each period, from S-ISM to WEC2. The Hg

414   monitoring data, meteorological factors, and pollutant data in Lhasa were statistically and

415   dimensionally reduced by PCA to analyze the relationships among them. The components related

416   to Hg were selected and analyzed separately for each period, and the principal components were

417   extracted (Table 4). According to the variable's loadings on each component, they were assigned as

418   Special Hg-related factor, Local emission factor, and Wind factor.

Table 4 PCA factor loadings (varimax rotated factor matrix) for Hg in Lhasa, China.

Tentative Identification	Special Hg-related			Local emission		Wind	
preiod	S-ISM	WEC1	WEC2	WEC1	WEC2	S-ISM	WEC2
GEM	**0.87**	**0.63**	**0.9**	0.44	0.3	-0.21	-0.13
PBM	**0.96**	**0.79**	**0.63**				
GOM	**0.95**	**0.87**	**0.95**	0.11	0.1		
Temp				-0.29	0.2		**0.92**
Hum		-0.19	0.17	-0.26	-0.18	-0.26	**-0.75**
Wind_Speed	-0.1	-0.14		-0.37		**0.87**	**0.91**
Rain							
Solar_Rad.				-0.21			
CO	0.17		0.11	**0.87**	**0.69**	-0.22	**0.51**
NO$_2$		0.13		**0.92**	**0.96**	-0.25	
O$_3$			-0.36	**-0.89**	**-0.83**	0.53	
PM$_{10}$	-0.14			**0.86**	**0.69**		0.14
PM$_{2.5}$	-0.16		0.16	**0.83**	**0.86**		
SO$_2$	0.26	0.17	**0.86**	**0.75**			
Variance Explained	19.6	13.69	21.88	35.13	24.94	9.25	18.32

Note: variables with high factor loadings (> 0:5) were marked in bold. For readability, variables with very low factor loadings (< 0:1) are not presented.

419

420 A special Hg-related factor (Factor 1) was assigned owing to the continuous high positive

421 loading of GEM, GOM, and PBM from the SISM to the WEC periods; only high positive loading

422 of SO$_2$ was found in the WEC2 period. For this factor, there was no significant relationship with

423 any other meteorological factors or pollutants. The high positive loading of this factor for all three

424 Hg species and the low correlation with meteorological factors and other pollutants may indicate

425 that this is a specific source of Hg. As the short transmission distance of the GOM and PBM, the

426 special Hg-related source should be closer to Lhasa. However, no particular source of Hg around

427 Lhasa has been reported in the literature, so the source indicated by this factor remains unclear.

428 Factor 2 had slight positive relationship with GEM and GOM, high positive loading of

429 CO/NO$_2$/PM$_{10}$/PM$_{2.5}$/SO$_2$, and high negative loading of O$_3$ during the WEC period. The high

430 positive loadings of CO/NO$_2$/PM$_{10}$/PM$_{2.5}$/SO$_2$ may indicate that this factor is highly correlated with

431 the combustion source. As O$_3$ concentration rapidly decreased after sunset (Figure 4. a), high

432 negative loading of O$_3$ further indicated that this factor represented events during the nighttime with

433   low O₃ concentrations. Since the WEC period overlapped with the heating season in Lhasa, Factor

434   2 may be strongly associated with heating combustion.

435   The wind factor (Factor 3) involves high positive loading of wind speed and low negative

436   loading of GEM concentration during the S-ISM and WEC2 periods. This factor reveals the

437   scavenging effect of wind on the local GEM in Lhasa. For high wind speed, the air masses with low

438   GEM concentrations in the surrounding area mixed with the air masses in Lhasa, leding to a

439   reduction in the GEM concentration. Concurrently, some GEM in Lhasa was carried away from the

440   city by wind. Factor 3 was consistent with the analysis of the wind effect on the diurnal variation of

441   Hg concentrations (Section 3.2), indicating the effect of strong winds on urban Hg removal.

442   **3.5   Atmospheric Hg source trajectories and potential source regions in the Lhasa area**

443   Figure 4 shows the GEM backward trajectory paths from the S-ISM period to the WEC2 period

444   in Lhasa. During the S-ISM period, most trajectories (cluster 1, representative GEM concentration

445   of 2.66 ng m^{-3}, 87.53% of the trajectory during this period, Table S1) originated from or passed

446   through the south of Lhasa. The source of the trajectory points directly to the Indian Ocean, likely

447   as these transported air masses are still subject to Indian monsoon action in September. According

448   to the UNEP Hg emission inventory (UNEP, 2013), there are few anthropogenic emissions along

449   this trajectory, indicating that the GEM may originate from the Indian Ocean or locally from Lhasa.

450   Clusters 2 and 3 may indicate the trajectories of air masses driven by westerly circulation, which

451   had a low proportion in the S-ISM period, with slightly different GEM concentrations from different

452   sources.

453   During the WEC1 period, the driving factor of the air mass gradually shifted from Indian

454   monsoon to westerly circulation. Clusters 2 and 3 are trajectories driven by the higher-height

455   westerly circulation during the WEC1 period with a higher proportion than in the S-ISM period.

456   Cluster 1 came from the southwest of Lhasa, and the air mass moved along the Himalayas before

457   entering the Tibetan Plateau and was transported to Lhasa. Compared to the S-ISM period, the GEM

458   concentration of this trajectory decreased slightly, which may be related to the source of the air mass

459   and the areas it passes through. WEC2 showed little change in trajectory sources compared to WEC1,

460   but all trajectory concentrations decreased significantly. Both WEC1 and WEC2 were in winter,

461   and both had similar trajectories related to the driving wind field. Significantly decreasing GEM

462   concentrations may suggest a local influence in Lhasa City. The local GEM in Lhasa consists of

463   background concentrations superimposed on local emissions, and the share of local emissions

464   decreases under better dispersion conditions (higher wind speeds) during the WEC2 period. The

465   GEM concentration during the WEC2 period in Lhasa is only 0.16 ng m^{-3}, higher than the

466   concentration during the WEC period in the QNNP region ($1:31 \pm 0:42$ ng m^{-3}) (Lin et al., 2019)).
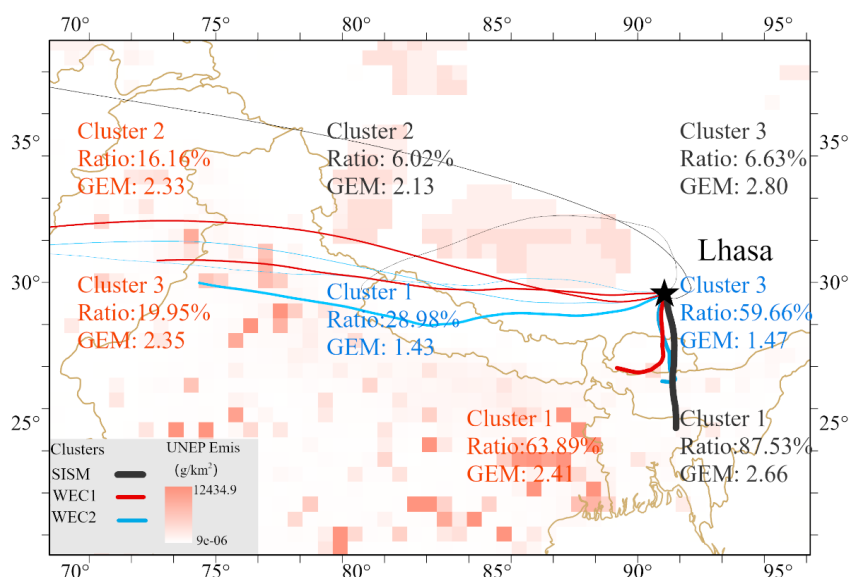
467   **Figure 5 Clusters of the back trajectory analysis from Lhasa during S-ISM and WEC**

468   **periods. The thickness of the line represents the ratio of the cluster in the time period, the**

469   **background is the global Hg emission inventory developed by UNEP (2013a).**

470   **3.6 Comparison of three typical sites on the Tibetan Plateau**

471   Different levels and variation patterns of Hg species concentrations were observed in the

472   Qomolangma National Nature Preserve (QNNP, 4,276 m) (Lin et al., 2019), Nyingchi (SET, 3,263

473   m) (Lin et al., 2022), and Lhasa (3,650 m) areas, which are typical monsoon-influenced, canyon,

474   and urban areas on the Tibetan Plateau, respectively. Predictably, Hg species concentrations were

475   generally lower on the Tibetan Plateau, while background areas with few populations on the Plateau

476   were lower than those on the plains in mainland China, and cities on the Plateau were lower than

477   those on the plains. Although the transboundary transport of pollutants has received considerable

478   notice (Huang et al., 2016b;Wang et al., 2018;Lin et al., 2019;Zhu et al., 2019;Feng et al., 2019),

Atmospheric
Chemistry
and Physics
Discussions

Open Access

EGU

479   the comparison between QNNP and Lhasa indicates that the contribution of local anthropogenic

480   sources may be significant for atmospheric pollutant concentrations. The comparison also suggests

481   that atmospheric Hg emissions from urban residential life may be an important source that can be

482   valuable in inventory studies.

483   Vastly different patterns of Hg species concentrations were found in the QNNP and SET due

484   to differences in geography and vegetation cover. Atmospheric Hg transported to QNNP is subject

485   to a combination of monsoonal action and the pumping effect of glacial winds. However,

486   atmospheric Hg entering the SET area has a slow elevation increasing path, and abundant

487   precipitation and vegetation have a significant trapping effect on atmospheric Hg. While for Lhasa,

488   a direct effect of local wind fields on the accumulation or rapid removal of GEM concentrations

489   was found. This suggests that although global transport is important in the Hg cycle, the pollution

490   at each location is likely to be strongly influenced by the local environment, even in exceptionally

491   clean areas such as the Tibetan Plateau. However, there are still relatively few studies on GOM and

492   PBM in the Tibetan Plateau, and more comprehensive investigations are required on how changes

493   in Hg speciation transformation on snow and ice surfaces affect the environment, the effect of

494   stratospheric intrusion on GOM concentrations (which is common on the Plateau), and the effect of

495   particulate matter on Hg(II) gas-particle partitioning, which would help to understand the Hg species

496   change on the Plateau and throughout the world.

497   **4. Conclusions**

498   Lhasa is the largest city on the Tibetan Plateau; thus, its atmospheric Hg concentrations

499   represent the highest level of atmospheric Hg pollution in this area. Unexpectedly high

500   concentrations of atmospheric mercury species were found in Lhasa. The GEM concentrations were

501   higher than the Northern Hemisphere background concentrations, and the GOM and PBM

502   concentrations were high among Chinese cities. Monitoring of atmospheric Hg in Lhasa showed

503   that the mean concentrations of GEM, GOM, and PBM during the S-ISM period (2.73 ± 1.48 ng m^{-3},

504   38.4 ± 62.7 pg m^{-3}, and 59.1 ± 181.0 pg m^{-3}, respectively) were higher than those during the WEC

505   period (2.11 ± 2.09 ng m^{-3}, 35.8 ± 43.3 pg m^{-3}, and 52.9 ± 90.1 pg m^{-3}, respectively). Combined

506   with the trajectory analysis, the high atmospheric Hg concentrations during the S-ISM phase may

507   have originated from external long-range transport.

508   Analysis of the overall concentration changes revealed some irregular and sudden high

509   atmospheric Hg concentration events in Lhasa. Analysis of these events suggests that local sources

510   (such as combustion events) can cause severely elevated concentration events under low wind

511   speeds and the presence of a low-height nighttime boundary layer. Analysis of the diurnal variation

512   of concentrations confirmed that low wind speeds and a low height nocturnal boundary layer would

513   lead to the elevated local Hg concentrations. In contrast, higher wind speeds could rapidly remove

514   atmospheric Hg from Lhasa. PCA analysis of the influencing factors indicates that local sources,

515   especially special Hg-related sources, are important factors influencing the variability of

516   atmospheric Hg. The PCA analysis also indicated the important role of higher wind speeds in

517   reducing atmospheric Hg concentrations in the urban areas of Lhasa, likely owing to the large Hg

518   concentration difference between Lhasa and surrounding areas.

519   Up to this study, we have obtained atmospheric Hg monitoring data from four typical areas of

520   the Tibetan Plateau: Lhasa, QNNP, SET, and Namco. The atmospheric Hg concentrations in the

521   background areas were at or below the average GEM concentration of Northern Hemisphere, with

522   higher levels in the urban area of Lhasa. Factors such as long-range transport of atmospheric

523   mercury, effects of local meteorological conditions, local glaciers, etc., were considered in these

524   studies. Further monitoring of additional areas and regional simulations are required to confirm the

525   atmospheric Hg transport patterns and fluxes.

526

532   **Data availability.** All the data presented in this paper can be made available for scientific

533   purposes upon request to the corresponding authors.

534   **Author contributions.** HL,XW, YT, QZ and XY designed the research and performed field

535   measurements. HL and YT performed the data analysis and model simulations. HL led the paper

536   writing. LC,CY, ZC, QZ, SK, JL, JS and BF contributed to the scientific discussion and the paper

537   preparation.

538   **Competing interests.** The authors declare that they have no conflict of interest.

539

References

- Brooks, S., Luke, W., Cohen, M., Kelly, P., Lefer, B., and Rappenglück, B. J. A. E.: Mercury species measured atop the Moody Tower TRAMP site, Houston, Texas, 44, 4045-4055, 2010.
- Chai, T., Stein, A., Ngan, F., and Draxler, R.: Inverse modeling with HYSPLIT Lagrangian Dispersion Model-Tests and Evaluation using the Cross Appalachian Tracer Experiment (CAPTEX) data, AGU Fall Meeting Abstracts, 2016.
- Chai, T., Crawford, A., Stunder, B., Pavolonis, M. J., Draxler, R., and Stein, A.: Improving volcanic ash predictions with the HYSPLIT dispersion model by assimilating MODIS satellite retrievals, Atmospheric Chemistry and Physics, 17, 2865-2879, 2017.
- Chen, P., Kang, S., Bai, J., Sillanpää, M., and Li, C.: Yak dung combustion aerosols in the Tibetan Plateau: Chemical characteristics and influence on the local atmospheric environment, Atmospheric Research, 156, 58-66, 10.1016/j.atmosres.2015.01.001, 2015.
- Cheng, I., Zhang, L., Blanchard, P., Graydon, J., St Louis, V. J. A. C., and Physics: Source-receptor relationships for speciated atmospheric mercury at the remote Experimental Lakes Area, northwestern Ontario, Canada, 12, 1903-1922, 2012.
- Cheng, M., Liu, M., Li, D., Luo, Q., Zhang, Z., Yuan, L., Yu, C., Xie, H., Lin, H., and Zhang, Q.: Human Methylmercury Exposure and Potential Impacts in Central Tibet: Food and Traditional Tibetan Medicine, Bulletin of Environmental Contamination and Toxicology, 1-10, 2021.
- Ci, Z., Zhang, X., Wang, Z., and Niu, Z.: Atmospheric gaseous elemental mercury (GEM) over a coastal/rural site downwind of East China: temporal variation and long-range transport, Atmospheric Environment, 45, 2480-2487, 2011.
- Cong, Z., Kang, S., Luo, C., Li, Q., Huang, J., Gao, S., and Li, X.: Trace elements and lead isotopic composition of PM10 in Lhasa, Tibet, Atmospheric Environment, 45, 6210-6215, 2011.
- Dommergue, A., Ferrari, C. P., Gauchard, P. A., Boutron, C. F., Poissant, L., Pilote, M., Jitaru, P., and Adams, F. C. J. G. r. l.: The fate of mercury species in a sub-arctic snowpack during snowmelt, 30, 2003.
- Duan, L., Wang, X., Wang, D., Duan, Y., Cheng, N., and Xiu, G.: Atmospheric mercury speciation in Shanghai, China, Science of the Total Environment, 578, 460-468, 2017.
- Feng, X., Fu, X., and Zhang, H.: Observations of atmospheric Hg species and depositions in remote areas of China, E3S Web of Conferences, 2013.
- Feng, X., and Fu, X.: Monsoon-facilitated characteristics and transport of atmospheric mercury at a high-altitude background site in southwestern China, Atmos. Chem. Phys, 1680, 7324, 2016.
- Feng, Y., Wang, W., and Liu, J. J. W.: Dilemmas in and Pathways to Transboundary Water Cooperation between China and India on the Yaluzangbu-Brahmaputra River, 11, 2096, 2019.
- Fu, X., Feng, X., Zhu, W., Wang, S., and Lu, J.: Total gaseous mercury concentrations in ambient air in the eastern slope of Mt. Gongga, South-Eastern fringe of the Tibetan plateau, China, Atmospheric Environment, 42, 970-979, 2008.
- Fu, X., Feng, X., Liang, P., Zhang, H., Ji, J., and Liu, P.: Temporal trend and sources of speciated atmospheric mercury at Waliguan GAW station, Northwestern China, Atmospheric Chemistry and Physics, 12, 1951-1964, 2012a.
- Fu, X., Feng, X., Sommar, J., and Wang, S.: A review of studies on atmospheric mercury in China, Science of the Total Environment, 421, 73-81, 2012b.
- Fu, X., Maruszczak, N., Heimbürger, L.-E., Sauvage, B., Gheusi, F., Prestbo, E. M., and Sonke, J.

584   E.: Atmospheric mercury speciation dynamics at the high-altitude Pic du Midi Observatory,
585   southern France, Atmos. Chem. Phys, 16, 5623-5639, 2016a.
586 · Fu, X., Zhu, W., Zhang, H., Sommar, J., Yu, B., Yang, X., Wang, X., Lin, C.-J., and Feng, X.:
587   Depletion of atmospheric gaseous elemental mercury by plant uptake at Mt. Changbai,
588   Northeast China, Atmospheric Chemistry and Physics, 16, 12861-12873, 2016b.
589 · Fu, X., Zhang, H., Feng, X., Tan, Q., Ming, L., Liu, C., Zhang, L. J. E. s., and technology: Domestic
590   and transboundary sources of atmospheric particulate bound mercury in remote areas of
591   China: evidence from mercury isotopes, 53, 1947-1957, 2019.
592 · Gay, D. A., Schmeltz, D., Prestbo, E., Olson, M., Sharac, T., and Tordon, R.: The Atmospheric
593   Mercury Network: measurement and initial examination of an ongoing atmospheric mercury
594   record across North America, Atmospheric Chemistry and Physics, 13, 11339-11349,
595   10.5194/acp-13-11339-2013, 2013.
596 · Gratz, L., Esposito, G., Dalla Torre, S., Cofone, F., Pirrone, N., and Sprovieri, F.: First
597   Measurements of Ambient Total Gaseous Mercury (TGM) at the EvK2CNR Pyramid
598   Observatory in Nepal, E3S Web of Conferences, 2013.
599 · Guo, J., Kang, S., Huang, J., Zhang, Q., Tripathee, L., and Sillanpää, M.: Seasonal variations of
600   trace elements in precipitation at the largest city in Tibet, Lhasa, Atmospheric Research, 153,
601   87-97, 2015.
602 · Hong, Q., Xie, Z., Liu, C., Wang, F., Xie, P., Kang, H., Xu, J., Wang, J., Wu, F., and He, P.: Speciated
603   atmospheric mercury on haze and non-haze days in an inland city in China, Atmospheric
604   Chemistry and Physics, 16, 13807-13821, 2016.
605 · Hu, Q. H., Kang, H., Li, Z., Wang, Y. S., Ye, P. P., Zhang, L. L., Yu, J., Yu, X. W., Sun, C., and Xie,
606   Z. Q.: Characterization of atmospheric mercury at a suburban site of central China from
607   wintertime to springtime, Atmospheric Pollution Research, 5, 769-778, 2014.
608 · Huang, J., Kang, S., Shen, C., Cong, Z., Liu, K., Wang, W., and Liu, L.: Seasonal variations and
609   sources of ambient fossil and biogenic-derived carbonaceous aerosols based on 14C
610   measurements in Lhasa, Tibet, Atmospheric Research, 96, 553-559, 2010.
611 · Huang, J., Kang, S., Wang, S., Wang, L., Zhang, Q., Guo, J., Wang, K., Zhang, G., and Tripathee,
612   L.: Wet deposition of mercury at Lhasa, the capital city of Tibet, Science of the total
613   environment, 447, 123-132, 2013.
614 · Huang, J., Kang, S., Guo, J., Zhang, Q., Cong, Z., Sillanpää, M., Zhang, G., Sun, S., and Tripathee,
615   L.: Atmospheric particulate mercury in Lhasa city, Tibetan Plateau, Atmospheric Environment,
616   142, 433-441, 2016a.
617 · Huang, J., Kang, S., Tian, L., Guo, J., Zhang, Q., Cong, Z., Sillanpää, M., Sun, S., and Tripathee,
618   L.: Influence of long-range transboundary transport on atmospheric water vapor mercury
619   collected at the largest city of Tibet, Science of The Total Environment, 566, 1215-1222, 2016b.
620 · Hurst, T., and Davis, C.: Forecasting volcanic ash deposition using HYSPLIT, Journal of Applied
621   Volcanology, 6, 5, 2017.
622 · Jackson, J. E.: A user's guide to principal components, John Wiley & Sons, 2005.
623 · Kellerhals, M., Beauchamp, S., Belzer, W., Blanchard, P., Froude, F., Harvey, B., McDonald, K.,
624   Pilote, M., Poissant, L., and Puckett, K.: Temporal and spatial variability of total gaseous
625   mercury in Canada: results from the Canadian Atmospheric Mercury Measurement Network
626   (CAMNet), Atmospheric Environment, 37, 1003-1011, 2003.
627 · Lan, X., Talbot, R., Castro, M., Perry, K., and Luke, W.: Seasonal and diurnal variations of

628   atmospheric mercury across the US determined from AMNet monitoring data, Atmospheric
629   Chemistry and Physics, 12, 10569-10582, 2012.
630 · Li, C., Bosch, C., Kang, S., Andersson, A., Chen, P., Zhang, Q., Cong, Z., Chen, B., Qin, D., and
631   Gustafsson, Ö.: Sources of black carbon to the Himalayan–Tibetan Plateau glaciers, Nature
632   Communications, 7, 12574, 2016a.
633 · Li, C., Chen, P., Kang, S., Yan, F., Hu, Z., Qu, B., and Sillanpää, M.: Concentrations and light
634   absorption characteristics of carbonaceous aerosol in PM2. 5 and PM10 of Lhasa city, the
635   Tibetan Plateau, Atmospheric Environment, 127, 340-346, 2016b.
636 · Li, J., Lin, T., Qi, S., Zhang, G., Liu, X., and Li, K.: Evidence of local emission of organochlorine
637   pesticides in the Tibetan plateau, Atmospheric Environment, 42, 7397-7404, 2008.
638 · Li, Y., Wang, Y., Li, Y., Li, T., Mao, H., Talbot, R., Nie, X., Wu, C., Zhao, Y., and Hou, C.:
639   Characteristics and potential sources of atmospheric particulate mercury in Jinan, China,
640   Science of The Total Environment, 574, 1424-1431, 2017.
641 · Lin, H., Tong, Y., Yin, X., Zhang, Q., Zhang, H., Zhang, H., Chen, L., Kang, S., Zhang, W., and
642   Schauer, J.: First measurement of atmospheric mercury species in Qomolangma Natural
643   Nature Preserve, Tibetan Plateau, and evidence oftransboundary pollutant invasion,
644   Atmospheric Chemistry and Physics, 19, 1373-1391, 2019.
645 · Lin, H., Tong, Y., Yu, C., Chen, L., Yin, X., Zhang, Q., Kang, S., Luo, L., Schauer, J., de Foy, B. J.
646   A. C., and Physics: First observation of mercury species on an important water vapor channel
647   in the southeastern Tibetan Plateau, 22, 2651-2668, 2022.
648 · Lindberg, S., Bullock, R., Ebinghaus, R., Engstrom, D., Feng, X., Fitzgerald, W., Pirrone, N.,
649   Prestbo, E., and Seigneur, C.: A synthesis of progress and uncertainties in attributing the
650   sources of mercury in deposition, AMBIO: a Journal of the Human Environment, 36, 19-33,
651   2007.
652 · Lindberg, S. a., and Stratton, W.: Atmospheric mercury speciation: concentrations and
653   behavior of reactive gaseous mercury in ambient air, Environmental Science & Technology,
654   32, 49-57, 1998.
655 · Liu, B., Keeler, G. J., Dvonch, J. T., Barres, J. A., Lynam, M. M., Marsik, F. J., and Morgan, J. T. J.
656   A. E.: Temporal variability of mercury speciation in urban air, 41, 1911-1923, 2007.
657 · Liu, N., Qiu, G., Landis, M. S., Feng, X., Fu, X., and Shang, L.: Atmospheric mercury species
658   measured in Guiyang, Guizhou province, southwest China, Atmospheric Research, 100, 93-
659   102, 2011.
660 · Liu, S., Nadim, F., Perkins, C., Carley, R. J., Hoag, G. E., Lin, Y., and Chen, L.: Atmospheric
661   mercury monitoring survey in Beijing, China, Chemosphere, 48, 97-107, 2002.
662 · Luo, Y., Duan, L., Driscoll, C. T., Xu, G., Shao, M., Taylor, M., Wang, S., and Hao, J. J. J. o. G. R.
663   B.: Foliage/atmosphere exchange of mercury in a subtropical coniferous forest in south China,
664   121, 2006-2016, 2016.
665 · Lynam, M. M., Dvonch, J. T., Hall, N. L., Morishita, M., and Barres, J. A.: Spatial patterns in wet
666   and dry deposition of atmospheric mercury and trace elements in central Illinois, USA,
667   Environmental Science and Pollution Research, 21, 4032-4043, 2014.
668 · Pant, N., Ravindra, R., Srivastava, D., and Thompson, L.: The Himalayan cryosphere: past and
669   present variability of the 'third pole', Geological Society, London, Special Publications, 462,
670   SP462. 413, 2018.
671 · Pokhrel, B., Gong, P., Wang, X., Gao, S., Wang, C., and Yao, T.: Sources and environmental

672   processes of polycyclic aromatic hydrocarbons and mercury along a southern slope of the
673   Central Himalayas, Nepal, Environmental Science and Pollution Research, 23, 13843-13852,
674   2016.
675 · Qiu, J.: China: the third pole, Nature News, 454, 393-396, 2008.
676 · Rhode, D., Madsen, D. B., Brantingham, P. J., and Dargye, T.: Yaks, yak dung, and prehistoric
677   human habitation of the Tibetan Plateau, Developments in Quaternary Sciences, 9, 205-224,
678   2007.
679 · Sallon, S., Namdul, T., Dolma, S., Dorjee, P., Dolma, D., Sadutshang, T., Ever-Hadani, P.,
680   Bdolah-Abram, T., Apter, S., and Almog, S.: Mercury in traditional Tibetan medicine-panacea
681   or problem?, Human & experimental toxicology, 25, 405-412, 2006.
682 · Seigneur, C., Vijayaraghavan, K., and Lohman, K.: Atmospheric mercury chemistry: Sensitivity
683   of global model simulations to chemical reactions, Journal of Geophysical Research:
684   Atmospheres, 111, 2006.
685 · Selin, N. E.: Global biogeochemical cycling of mercury: a review, Annual Review of
686   Environment and Resources, 34, 43, 2009.
687 · Slemr, F., Angot, H., Dommergue, A., Magand, O., Barret, M., Weigelt, A., Ebinghaus, R.,
688   Brunke, E.-G., Pfaffhuber, K. A., and Edwards, G.: Comparison of mercury concentrations
689   measured at several sites in the Southern Hemisphere, Atmospheric Chemistry and Physics,
690   15, 3125-3133, 2015.
691 · Song, S., Angot, H., Selin, N. E., Gallée, H., Sprovieri, F., Pirrone, N., Helmig, D., Savarino, J.,
692   Magand, O., and Dommergue, A.: Understanding mercury oxidation and air–snow exchange
693   on the East Antarctic Plateau: a modeling study, 2018.
694 · Sprovieri, F., Gratz, L., and Pirrone, N.: Development of a ground-based atmospheric
695   monitoring network for the Global Mercury Observation System (GMOS), E3S Web of
696   Conferences, 2013.
697 · Sprovieri, F., Pirrone, N., Bencardino, M., D'Amore, F., Carbone, F., Cinnirella, S., Mannarino,
698   V., Landis, M., Ebinghaus, R., and Weigelt, A.: Atmospheric mercury concentrations observed
699   at ground-based monitoring sites globally distributed in the framework of the GMOS network,
700   Atmospheric Chemistry and Physics, 16, 11915-11935, 2016.
701 · Steffen, A., Douglas, T., Amyot, M., Ariya, P., Aspmo, K., Berg, T., Bottenheim, J., Brooks, S.,
702   Cobbett, F., and Dastoor, A.: A synthesis of atmospheric mercury depletion event chemistry
703   in the atmosphere and snow, Atmospheric Chemistry and Physics, 8, 1445-1482, 2008.
704 · Stein, A., Draxler, R. R., Rolph, G. D., Stunder, B. J., Cohen, M., and Ngan, F.: NOAA's HYSPLIT
705   atmospheric transport and dispersion modeling system, Bulletin of the American
706   Meteorological Society, 96, 2059-2077, 2015.
707 · Stylo, M., Alvarez, J., Dittkrist, J., and Jiao, H.: Global review of mercury monitoring networks,
708   UNEP, Geneva, 2016.
709 · Swartzendruber, P., Jaffe, D., and Finley, B.: Improved fluorescence peak integration in the
710   Tekran 2537 for applications with sub-optimal sample loadings, Atmospheric Environment,
711   43, 3648-3651, 2009.
712 · Tibet Bureau of Statistics, T.: Tibet Statistics Yearbook, China Statistics Press, Beijing, 2020.
713 · Travnikov, O., Angot, H., Artaxo, P., Bencardino, M., Bieser, J., D'Amore, F., Dastoor, A., Simone,
714   F. D., Diéguez, M. d. C., and Dommergue, A.: Multi-model study of mercury dispersion in the
715   atmosphere: atmospheric processes and model evaluation, Atmospheric Chemistry and

716   Physics, 17, 5271-5295, 2017.

717   · UNEP, U. G. M. A.: Sources, Emissions, Releases and Environmental Transport; UNEP
718   Chemicals Branch: Geneva, Switzerland, 2013, There is no corresponding record for this
719   reference, 2013.

720   · Venter, A., Beukes, J., Van Zyl, P., Brunke, E.-G., Labuschagne, C., Slemr, F., Ebinghaus, R., and
721   Kock, H.: Statistical exploration of gaseous elemental mercury (GEM) measured at Cape Point
722   from 2007 to 2011, Atmospheric Chemistry and Physics, 15, 10271-10280, 2015.

723   · Wang, C., Wang, X., Gong, P., and Yao, T.: Long-term trends of atmospheric organochlorine
724   pollutants and polycyclic aromatic hydrocarbons over the southeastern Tibetan Plateau,
725   Science of the Total Environment, 624, 241-249, 2018.

726   · Wang, X., Zhang, H., Lin, C. J., Fu, X., Zhang, Y., and Feng, X.: Transboundary transport and
727   deposition of Hg emission from springtime biomass burning in the Indo-China Peninsula,
728   Journal of Geophysical Research: Atmospheres, 120, 9758-9771, 2015.

729   · Xiao, Q., Saikawa, E., Yokelson, R. J., Chen, P., Li, C., and Kang, S.: Indoor air pollution from
730   burning yak dung as a household fuel in Tibet, Atmospheric Environment, 102, 406-412,
731   10.1016/j.atmosenv.2014.11.060, 2015.

732   · Yang, J., Kang, S., Ji, Z., and Chen, D.: Modeling the origin of anthropogenic black carbon and
733   its climatic effect over the Tibetan Plateau and surrounding regions, Journal of Geophysical
734   Research: Atmospheres, 123, 671-692, 2018.

735   · Yang, Y., Chen, H., and Wang, D.: Spatial and temporal distribution of gaseous elemental
736   mercury in Chongqing, China, Environmental monitoring and assessment, 156, 479-489, 2009.

737   · Yao, T., Thompson, L. G., Mosbrugger, V., Zhang, F., Ma, Y., Luo, T., Xu, B., Yang, X., Joswiak,
738   D. R., and Wang, W.: Third pole environment (TPE), Environmental Development, 3, 52-64,
739   2012.

740   · Yin, X., Kang, S., Foy, B. d., Ma, Y., Tong, Y., Zhang, W., Wang, X., Zhang, G., and Zhang, Q.:
741   Multi-year monitoring of atmospheric total gaseous mercury at a remote high-altitude site
742   (Nam Co, 4730 m asl) in the inland Tibetan Plateau region, Atmospheric Chemistry and
743   Physics, 18, 10557-10574, 2018.

744   · Yin, X., Zhou, W., Kang, S., de Foy, B., Yu, Y., Xie, J., Sun, S., Wu, K., and Zhang, Q.: Latest
745   observations of total gaseous mercury in a megacity (Lanzhou) in northwest China, Science
746   of The Total Environment, 720, 137494, 2020a.

747   · Yin, X., Zhou, W., Kang, S., de Foy, B., Yu, Y., Xie, J., Sun, S., Wu, K., and Zhang, Q. J. S. o. T. T.
748   E.: Latest observations of total gaseous mercury in a megacity (Lanzhou) in northwest China,
749   720, 137494, 2020b.

750   · Zhang, H., Fu, X., Lin, C., Wang, X., and Feng, X.: Observation and analysis of speciated
751   atmospheric mercury in Shangri-La, Tibetan Plateau, China, Atmos. Chem. Phys, 15, 653-665,
752   2015a.

753   · Zhang, H., Fu, X., Lin, C.-J., Shang, L., Zhang, Y., Feng, X., and Lin, C.: Monsoon-facilitated
754   characteristics and transport of atmospheric mercury at a high-altitude background site in
755   southwestern China, Atmospheric Chemistry & Physics, 16, 2016.

756   · Zhang, L., Wang, S., Wang, L., and Hao, J.: Atmospheric mercury concentration and chemical
757   speciation at a rural site in Beijing, China: implications of mercury emission sources,
758   Atmospheric Chemistry and Physics, 13, 10505-10516, 2013.

759   · Zhang, R., Wang, H., Qian, Y., Rasch, P. J., Easter, R. C., Ma, P.-L., Singh, B., Huang, J., and Fu,

760   Q.: Quantifying sources, transport, deposition, and radiative forcing of black carbon over the
761   Himalayas and Tibetan Plateau, Atmospheric Chemistry and Physics, 15, 6205-6223, 2015b.
762 · Zhou, H., Hopke, P. K., Zhou, C., and Holsen, T. M. J. S. o. t. T. E.: Ambient mercury source
763   identification at a New York State urban site: Rochester, NY, 650, 1327-1337, 2019.
764 · Zhu, J., Wang, T., Talbot, R., Mao, H., Hall, C., Yang, X., Fu, C., Zhuang, B., Li, S., and Han, Y.:
765   Characteristics of atmospheric total gaseous mercury (TGM) observed in urban Nanjing,
766   China, Atmospheric Chemistry and Physics, 12, 12103-12118, 2012.
767 · Zhu, J., Xia, X., Che, H., Wang, J., Cong, Z., Zhao, T., Kang, S., Zhang, X., Yu, X., Zhang, Y. J. A.
768   C., and Physics: Spatiotemporal variation of aerosol and potential long-range transport
769   impact over the Tibetan Plateau, China, 19, 14637-14656, 2019.